EIT reconstructions with improved spatial resolution based on FOCUSS method for a cylindrical model meshed by tri-prism elements

Guoya Dong, Xian Li, Hongyan Li, Manling Ge
Biomedical Engineering Department, School of Electrical Engineering,
Hebei University of Technology, Tianjin, 300130, CHINA
dongguoya@gmail.com

Abstract

This paper is aimed to reconstruct the EIT images with improved spatial resolution by a method based on FOCUSS for a cylindrical model meshed into tri-prism elements. The forward computations are carried out by the analytical method and the finite element method (FEM) for tri-prism elements respectively. By the comparisons between the numerical and analytical solutions, the precision of results based on FEM are estimated. Using the sensitive matrix method to construct the system matrix, initial estimations with low spatial resolution are solved by TSVD and sLORETA methods for the inverse problem, respectively. FOCUSS method is further adopted to improve the spatial resolution with the initial estimations from TSVD and sLORETA.

Key words: EIT, FOCUSS, sLORETA, spatial resolution, cylindrical model, tri-prism element

1. Introduction

In order to improve the spatial resolution of EIT images, FOCUSS method has been applied for 3-D spherical and realistic head model with tetrahedral meshes [1-3]. In this paper, the cylindrical model meshed into tri-prism elements are constructed for EIT reconstruction. In section 2, both numerical solutions by FEM and analytical solutions are achieved for EIT forward problem and comparisons are carried out to verify the efficiency of numerical solutions. In section 3, FOCUSS method are described in detail and reconstructed images with improved spatial resolution are obtained with tri-prism mesh for the cylindrical model.

2. Forward problem

2.1 Governing equations

Considering the boundary conditions, the potential-current relationship is determined by the Laplace equation (1). where σ is the conductivity, φ_0 is the electric potential at the given boundary, J_n is the injected current density at the fixed boundary.

$$\begin{cases} \Omega: \ \nabla \cdot \sigma \nabla \varphi = 0 \\ \Gamma_1: \ \varphi = \varphi_0 \\ \Gamma_2: \ \sigma \dfrac{\partial \varphi}{\partial n} = -J_n \end{cases} \tag{1}$$

2.2 Numerical solutions by FEM

Equation (2) can be derived [4], where $S=[S_{ij}]$ is the coefficient matrix, $F=[F_1,F_2,...,F_n]^T$ is relative to the injected current on the boundary, φ is potentials at nodes.

$$S\varphi = F \tag{2}$$

One tri-prism element is shown in Fig.1(a). The coefficient matrix for each element is obtained as (3) and (4)

$$S_{ij}^{e}=\sigma^{e}[\frac{h}{16\Delta}(1+\frac{\xi_i\xi_j}{3})q_iq_j+\frac{h}{16\Delta}(1+\frac{\xi_i\xi_j}{3})r_ir_j]+\begin{cases}\sigma^{e}\dfrac{\xi_i\xi_j\Delta}{6h} & (j=i/i')\\ \sigma^{e}\dfrac{\xi_i\xi_j\Delta}{12h} & (j\neq i/i')\end{cases} \qquad i,j=K,\ M,N,\ K',\ M',N' \tag{3}$$

where h and σ^e are the height and conductivity of each tri-prism element, respectively. By integrating the coefficient matrix S_{ij}^{e} of each element, the coefficient matrix S is obtained.

$$\begin{cases} p_K = x_M y_N - y_M x_N & p_M = x_N y_K - y_N x_K & p_N = x_K y_M - y_K x_M \\ q_K = y_M - y_N & q_M = y_N - y_K & q_N = y_K - y_M \\ r_K = x_N - x_M & r_M = x_K - x_N & r_N = x_M - x_K \end{cases} \tag{4}$$

$$\xi_{i,j} = \begin{cases} -1 & (i,j = K, M, N) \\ 1 & (i,j = K', M', N') \end{cases}, \qquad \Delta = \frac{1}{2}(q_K r_M - q_M r_K)$$

F_i^e is the current vector of nodes for each element as (5), right hand item $F = [F_1, F_2, ..., F_n]^T$ is obtained by integrating the F_i^e of all elements.

$$F_i^e = \begin{cases} -I/4 & \text{(at the nodes with current injected into)} \\ I/4 & \text{(at the nodes with current injected out)} \\ 0 & \text{(at the nodes without current injected)} \end{cases} \tag{5}$$

2.3 Analytical solutions

The geometry of the finite circular cylinder with two electrodes attached on its surface is shown in Fig.1 (b). The analytical solution of the potential is given by [5]:

$$\phi(\rho,\theta,z) = \frac{-4Ic}{\sigma\pi^3\Delta s(1+\delta_{0n})}\sum_{n=0}^{\infty}\frac{1}{n}\left\{\sum_{r=1}^{\infty}\frac{1}{r^2}\sin(\frac{r\pi s}{2c})\left[\cos(\frac{r\pi z1}{c})\cos(n(\theta-\theta_1)) - \cos(\frac{r\pi z2}{c})\cos(n(\theta-\theta_2))\right]\frac{I_n(\frac{r\pi\rho}{c})}{I_n'(\frac{r\pi a}{c})}\cos(\frac{r\pi z}{c})\right\}\sin(\frac{n\Delta}{2a})$$

$$-\frac{4Ic}{\sigma\pi^3\Delta s(1+\delta_{0n})}\sum_{n=0}^{\infty}\frac{1}{n}\left\{\sum_{r=0}^{\infty}\frac{1}{(\frac{2r+1}{2})^2}\sin(\frac{(2r+1)\pi s}{4c})\times\left[\sin(\frac{(2r+1)\pi z1}{2c})\cos(n(\theta-\theta_1)) - \sin(\frac{(2r+1)\pi z2}{2c})\cos(n(\theta-\theta_2))\right]\right. \tag{6}$$

$$\left.\bullet\frac{I_n(\frac{(2r+1)\pi\rho}{2c})}{I_n'(\frac{(2r+1)\pi a}{2c})}\sin(\frac{(2r+1)\pi z}{2c})\right\}\sin(\frac{n\Delta}{2a}) - \frac{Ia}{\sigma\pi\Delta c}\sum_{n=1}^{\infty}\frac{1}{n^2}(\frac{\rho}{a})^n\sin(\frac{n\Delta}{2a})\left[\cos(n(\theta-\theta_1)) - \cos(n(\theta-\theta_2))\right].$$

where $\delta_{0n} = \begin{cases} 1 & n=0 \\ 0 & n\neq 0 \end{cases}$, I is the injected current, σ is the conductivity and $\Delta = \frac{w}{2a}$, I_n is the modified Bessel function of the first kind and I_n' is the derivative of the modified Bessel function of the first kind.

The electric field is given as (7):

$$E = -\nabla\phi = -\frac{\partial\phi}{\partial\rho}\hat{e}_\rho - \frac{\partial\phi}{\rho\partial\theta}\hat{e}_\theta - \frac{\partial\phi}{\partial z}\hat{e}_z \tag{7}$$

Based on the transformation relationship between Cartesian coordinate system and cylindrical coordinate system [6], the electric field is given by

$$E = -\nabla\varphi = -\frac{\partial\varphi}{\partial x}\hat{e}_x - \frac{\partial\varphi}{\partial y}\hat{e}_y - \frac{\partial\varphi}{\partial z}\hat{e}_z = (-\frac{\partial\varphi}{\partial x}\cos\theta - \frac{\partial\varphi}{\partial y}\sin\theta)\hat{e}_\rho + (\frac{\partial\varphi}{\partial x}\sin\theta - \frac{\partial\varphi}{\partial y}\cos\theta)\hat{e}_\theta - \frac{\partial\varphi}{\partial z}\hat{e}_z \tag{8}$$

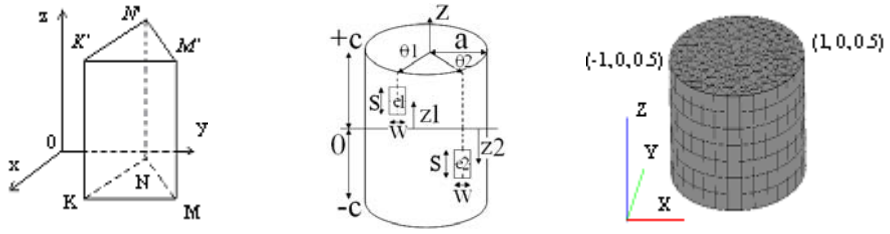

(a) (b) (c)

Fig.1 (a) A tri-prism element (b) Parameters of Cylinder (c) A cylinder model

2.4 Simulations

A homogenous uniform cylindrical model with a height of 1cm and radius of 1cm is shown in Fig.1(c). It is divided into seven layers including 1288 nodes and 2016 elements. With the analytical solution as a reference, the relative error is defined as (9)

$$e_r = \frac{\left|\varphi_{num} - \varphi_{ana}\right|}{\left|\varphi_{ana\_\max} - \varphi_{ana\_\min}\right|} \times 100\% \tag{9}$$

where φ_{num} is the potential solution by FEM and φ_{ana} is the analytical solution, $\varphi_{ana\_\max}$ and $\varphi_{ana\_\min}$ are the maximum and minimum potentials of the analytical solutions, respectively.

Sixteen rectangular electrodes are uniformly arranged around the boundary of the middle layer. The currents are injected through two opposite electrodes covered the two surface rectangle elements. One is enclosed by nodes 113, 114, 145 and 146, the other by nodes 97, 98, 129 and 130. The potentials of boundary nodes are displayed from the top to the bottom layer and an anticlockwise route around the boundary from (-1, 0) for each layer. The potential comparison between analytical solution and FEM solution is shown in Fig.2 (a). The potential errors of nodes near the electrode position are large. The maximum error is below 3.5%.

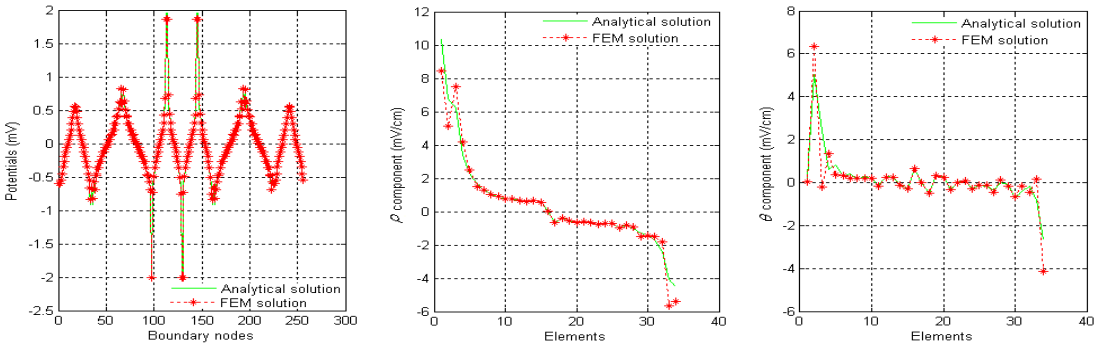

(a) (b) (c)

Fig.2 (a) Potentials of boundary nodes (b) ρ components of electric fields (c) θ components of electric fields

The electric field of each tri-prism element center is calculated respectively by using analytical and numerical methods. For the large number of elements, only are the elements across *X*-axis in the fourth plane displayed with the order along the *X* direction, shown in Fig.2 (b) and Fig.2 (c). The maximum errors of the ρ components and the θ component except a few points near the electrodes are below 6%. As for the *Z* components of the electric fields, the relative errors are less than 10^{-5}.

3. Image reconstructions

3.1 Linear Sensitivity Matrix

Linear sensitivity matrix *S* reflects the relationship between the conductivity change in each element C_p and the change of the boundary voltage U_p. In order to reduce the influence of electrode positioning error and measurement error on the reconstruction results, (10) can be normalized before the inverse. In this paper, TSVD and sLORETA methods are adopted for solving the linear inverse problem in order to obtain the initial estimations of reconstructed images [1,2].

$$U_p = SC_p \tag{10}$$

3.2 FOCUSS method

FOCUSS method, based on a low-resolution solution as the initial distribution, is a re-weighted minimum norm algorithm [7]. It is computed as (11), where *W* is a $m \times m$ matrix that provides a constraint on a weighting of the solution, which in turn causes the enhancement of some of the elements in *X*. Each step of the FOCUSS algorithm varies only in the weight matrix *X*. To enhance some of the already prominent elements, *W* can be constructed by taking the previous estimation as its diagonal elements, and then (11) is re-calculated. The two steps are repeated until the solution *X* no

$$\hat{X} = WW^T F^T (FWW^T F^T)^{-1} Y \tag{11}$$

longer changes, indicating that the algorithm has converged.

In 3D EIT, more elements increase the size of the weighting matrix as well as the computation time. In order to solve this problem, the shrinking FOCUSS method is utilized to shrink both the solution space and the weighting matrix in each iteration [2].

3.3 Reconstructed Images

Ninety-six measurement pairs are carried out with a diametric current injection and adjacent measurement (opposite-adjacent pattern). One perturbed region with the conductivity reduced by 60% is located in the fourth layer. The initial estimations reconstructed by TSVD and sLORETA are shown in Fig.3 (b). Followed by the shrinking FOCUSS method, the reconstructed images are achieved with the improved spatial resolution. Taking advantages of the smoother initial estimation from sLORETA, the reconstructed result by shrinking FOCUSS is better than that with initial estimation from TSVD. Therefore, initial estimations from sLORETA are applied for the shrinking FOCUSS method for two perturbations.

There are two perturbed regions with the conductivity reduced by 60% located in the fourth layer. They are moved from the boundary to the center region gradually, shown in Fig.4 (a). With the process of moving to the center, the initial estimations from sLORETA are not able to distinguish these two perturbations, shown in Fig.4 (b), while the results by shrinking sLORETA-FOCUSS can distinguish

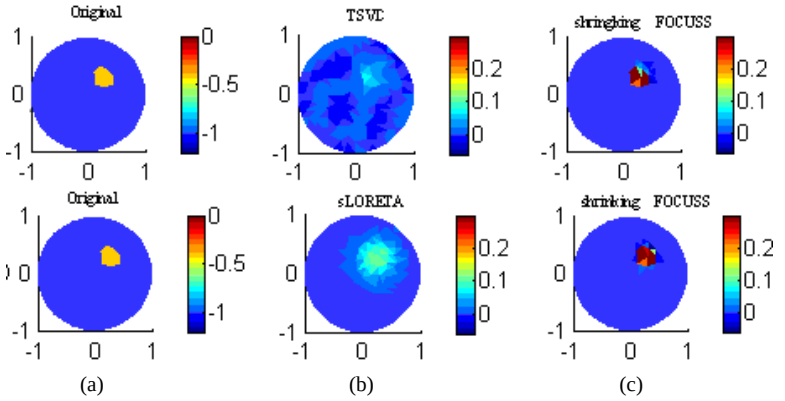

Fig.3 Reconstructed images (a) original distributions (b) initial estimations (c) reconstructed images by shrinking FOCUSS method

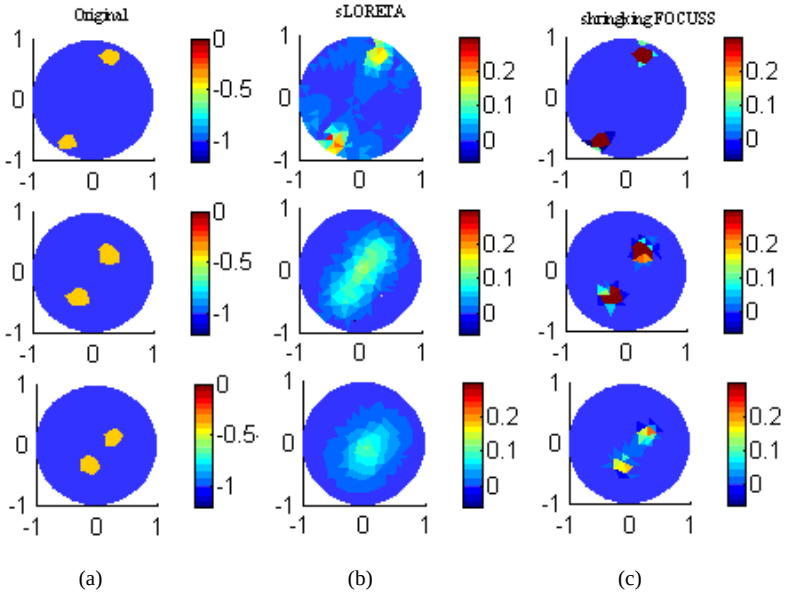

Fig.4 Image with the change of distance from the perturbation to the center (a) distance 0.8 (b) distance 0.5 (c) distance 0.3

them clearly, shown in Fig.4 (c).

4. Conclusions

This paper demonstrates the efficiency of numerical method by FEM for tri-prism meshes which has advantages for the computation of anisotropy media. By adopting smoother initial estimation from sLORETA, the spatial resolution improved EIT images are reconstructed by shrinking sLOREAT-FOCUSS method. In the future research, the anisotropy conductivity model will be used with the tri-prism mesh system.

References

[1] Guoya Dong, Hesheng Liu, Richard Bayford, et al. The spatial resolution improvement of EIT images by GVSPM-FOCUSS algorithm. *Physiol. Meas.* 2004, 25: 209-225.

[2] Guoya Dong, Hesheng Liu, Richard Bayford, et al. Spatial resolution improvement of 3D EIT images by the shrinking sLORETA-FOCUSS algorithm. *Physiol.Meas.* 2005, 26: S199-S208.

[3] Guoya Dong, Richard Bayford, Hesheng Liu, et al. EIT images with improved spatial resolution using a realistic head model. *28th Annual international conference of the IEEE Engineering in Medicine and biology society, New York City, USA, Aug30 - Sept 3 (EMBS'06).* 2006, 1134-1137.

[4] Guizhi Xu, Ying Li, Shuo Yang, et al. Electrical Impedance Tomography in Biomedical Engineering. *CHINA MACHINE PRESS.* 2010.

[5] F Kleinermann, N J Avis, and F A Alhargan. Analytical solution to the three-dimensional electrical forward problem for a circular cylinder. *Inverse problems.* 2000, 16: 461-468.

[6] Yanfeng Lu, Jianjun Liu, and Hongyan Lu. The Formulas of $\nabla\phi$. $\nabla \bullet A$. $\nabla \times A$ and ∇^2 in the Cylindrical and Spherical Coordinates. *Journal of Huaibei Normal University.* 2011, 32(1): 37-40.

[7] Irina F.Gorodnitsky, John S.George, and Bhaskar D.Rao. Neuromagnetic source imaging with FOCUSS: a recursive weighted minimum norm algorithm. *Electroencephalography and clinical Neurophysiology.* 1995, 95: 231-251.